

Discrete Sliding Mode control of small UAS in tight formation flight under information constraints

Jan Bolting* Soheib Fergani** Jean-Marc Biannic***
Francois Defay?? Martin Stolle??

* *National Institute of Standards and Technology, Boulder, CO 80305
USA (e-mail: author@boulder.nist.gov).*

** *Colorado State University, Fort Collins, CO 80523 USA (e-mail:
author@lamar.colostate.edu)*

*** *Electrical Engineering Department, Seoul National University,
Seoul, Korea, (e-mail: author@snu.ac.kr)*

!!! DRAFT !!!
Thursday 25th February, 2016
21:26

Abstract: This paper is concerned with a new control strategy based on discrete sliding mode control of small Unmanned Aerial Systems (UAS) in tight formation flight under information constraints. It addresses the problem of managing and coordinating several UAS to fly in a tight control formation. Since the formation of n UAS to be controlled is considered to fly in an arbitrary pattern in this work, a high-performance relative position control becomes an important issue. Indeed, a robust control strategy based on the sliding mode approach is proposed to achieve the desired flight performances while assuming realistic information constraints imposed by limited communication bandwidth and availability of relative localization sensors and preserving scalability with respect to formation size.

Also, this paper presents a meaningful study and comparison of the discrete sliding mode control design (DSMC) and time sampling continuous sliding mode control (TSCSMC). Indeed, it is important to study the performance differences between the two approaches that allow to choose the best strategy to be used to solve the considered problem. Here, the comparison focuses on the effect of the sampling on the control error, the mesh stability analytically and the mesh stability in simulation.

Simulation results of a flight scenario with two different sampling frequencies proves the efficiency of the proposed control strategy and shows clearly the effect of the discretization and the sampling on the formation flight behaviour of the UAS obtained by the chosen considered control.

Keywords: Flight formation, Aerospace unmanned vehicle, sliding mode control.

1. INTRODUCTION

Tight formation flight of aircraft can enable energy savings thanks to aerodynamic performance gains. The benefits of tight formation flight for bird-sized aircraft have been studied theoretically as early as in Hummel (1982). Both later theoretical (?), wind-tunnel results (?) and flight tests with manned aircraft consistently confirm energy savings of the order of 10%.

Numerous other applications such as distributed aerial imaging benefit from accurate relative position holding.

Enabling tight formation flight for small UAS is interesting for a number of reasons. Firstly, small UAS can serve as an inexpensive testbed for larger aircraft. Secondly,

small electrically driven UAS suffer from poor operational ranges.

Riding the wake of another aircraft, the follower is subject to large unknown wake disturbances. Sliding mode control provides robustness against large unknown perturbations.

Sliding mode control has successfully been applied to ground vehicle platooning (?). Higher order sliding mode has been proposed for UAS formation flight by Galzi and Shtessel (2006).

, DSMC, ACC on HOSMC for formations, applications of SMC for vehicle platoons

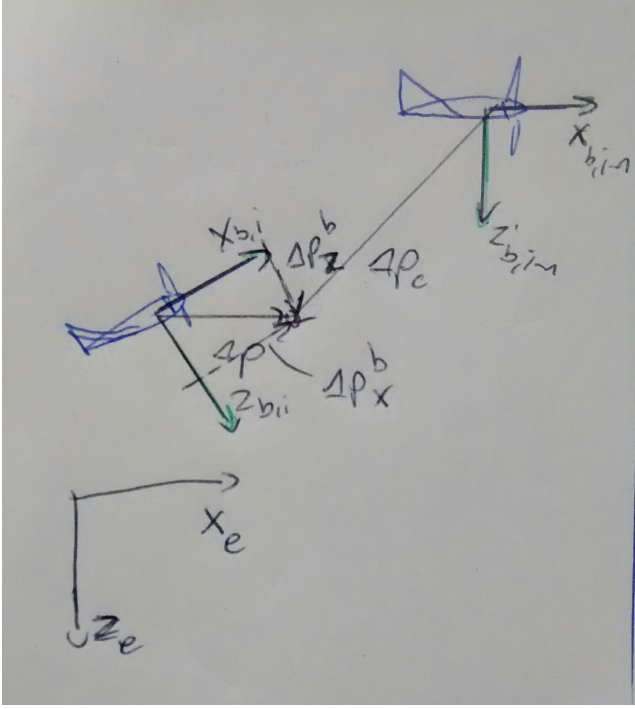


Fig. 1. Predecessor-follower geometry longitudinal

2. MODEL

2.1 Coordinate frames

The system to be controlled is a formation of n UAS flying in an arbitrary pattern. It is assumed that load factors are controlled in each vehicle's body frame (index b). Therefore separation errors are transformed into the body frame for control purposes, decoupling the three axes. The dynamics of each vehicle are defined in a local inertial North-East-Down frame (index e).

To dispose of a common reference frame for multiple members of the formation, the **Leader Speed Frame** (index ls) is defined. Its x axis is aligned with the formation leader's NED speed projected on the horizontal plane, its z axis is aligned with the NED frame's z axis, and its y axis completes a right-handed Cartesian coordinate system. It is used to define the separation vectors that make up the formation.

2.2 Vehicle Model

The continuous time vehicle position dynamics w.r.t. the local inertial frame are given by

$$\mathbf{x} = (\mathbf{p} \ \mathbf{v})^T \quad (1)$$

$$\dot{\mathbf{p}} = \mathbf{v} \quad (2)$$

$$\dot{\mathbf{v}} = \mathbf{a}_c + \mathbf{a}_w + \mathbf{g} \quad (3)$$

where $\mathbf{p} \in \mathbb{R}^3$ is the vehicle position, $\mathbf{v} \in \mathbb{R}^3$ is its velocity w.r.t. to the local inertial frame, $\mathbf{a}_w \in \mathbb{R}^3$ are accelerations induced by exogenous disturbances such as turbulence and another aircraft's wake, $\mathbf{a}_c \in \mathbb{R}^3$ are commanded accelerations and $\mathbf{g} \in \mathbb{R}^3$ is the gravity vector in the local inertial frame.

It is assumed that load factors \mathbf{n}_c are tracked by fast inner loop controllers in the vehicle body frame, leading to actual load factors $\mathbf{n} = \mathbf{n}_c + \mathbf{n}_w$ where $\mathbf{n}_w = \frac{1}{|\mathbf{g}|} \mathbf{a}_w$ are parasitic load factors introduced by exogenous disturbances and imperfect tracking. This leads to

$$\dot{\mathbf{v}} = \mathbf{R}_{eb} |\mathbf{g}| \mathbf{n}_c + \mathbf{a}_w + \mathbf{g} \quad (4)$$

where $\mathbf{R}_{eb} \in \mathbb{R}^{3 \times 3}$ is the rotation matrix from the body frame to the local inertial frame and $\mathbf{n}_c = \frac{1}{|\mathbf{g}|} \mathbf{a}_c$ are commanded load factors. To simplify notation, it is assumed that the vehicle is trimmed, i.e. the nominal gravitational acceleration is compensated for by a trim control input $\mathbf{n}_{c,0} = \mathbf{R}_{be} (0 \ 0 \ -1)^T$ and a virtual control input is defined as

$$\mathbf{u} = \mathbf{R}_{eb} |\mathbf{g}| (\mathbf{n}_c - \mathbf{n}_{c,0}) \quad (5)$$

leading to

$$\dot{\mathbf{v}} = \mathbf{R}_{eb} |\mathbf{g}| \left(\frac{1}{|\mathbf{g}|} (\mathbf{R}_{be} \mathbf{u} + \mathbf{n}_{c,0}) \right) + \mathbf{a}_w + \mathbf{g} \quad (6)$$

$$\dot{\mathbf{v}} = \mathbf{u} + \mathbf{a}_w \quad (7)$$

where now \mathbf{a}_w also includes the small effects of imperfect knowledge of local gravitation. ???doubledefinition

Saturations on the virtual control input (27) can be derived from (15) as

$$|\mathbf{u}| \leq \mathbf{U} \quad (8)$$

$$\mathbf{U} = \mathbf{R}_{eb} |\mathbf{g}| (\mathbf{N} - \mathbf{n}_{c,0}) \quad (9)$$

Considering two UAS i and $i-1$, this leads to relative position error dynamics

$$\Delta \mathbf{p} = \mathbf{p}_i - \mathbf{p}_{i-1} - \Delta \mathbf{p}_c \quad (10)$$

$$\Delta \dot{\mathbf{p}} = \mathbf{v}_i - \mathbf{v}_{i-1} - \Delta \dot{\mathbf{p}}_c \quad (11)$$

$$\Delta \dot{\mathbf{v}} = \mathbf{a}_i - \mathbf{a}_{i-1} - \Delta \ddot{\mathbf{p}}_c \quad (12)$$

$$= \mathbf{a}_{c,i} + \mathbf{a}_{w,i} - \mathbf{a}_{i-1} - \Delta \ddot{\mathbf{p}}_c \quad (13)$$

$$= \mathbf{u} + \mathbf{a}_{w,i} - \mathbf{a}_{i-1} - \Delta \ddot{\mathbf{p}}_c \quad (14)$$

where $\Delta \mathbf{p}$ is the relative position error between UAS i and its predecessor $i-1$, $\Delta \mathbf{v}$ is the corresponding relative velocity error, $\Delta \mathbf{p}_c$ is the desired relative position to the predecessor, \mathbf{a} are accelerations.

The presented model is essentially of the same type as that used in Galzi and Shtessel (2006) and provides the benefit of being vehicle-agnostic, as the specific vehicle dynamics are covered by the inner loop load factor controllers. On the other hand, perturbations \mathbf{a}_w and control input saturations are specific to a given vehicle and mission environment. It covers rotary wings as well as fixed wing UAS, which are the focus of this work.

Formation geometry The trajectory of the formation w.r.t. the local inertial frame is defined by the nominal trajectory of a virtual leader aircraft. Arbitrary shapes of

the formation can be defined by the relative separation vectors $\Delta \mathbf{p}$.

3. CONTROL DESIGN

To benefit from significant aerodynamic performance gains, a follower aircraft needs to stay within a narrow spatial window roughly defined by (see e.g. Jake et al. (2003))

$$\begin{aligned} -0.2b < \Delta y' < -0.1b \\ -0.1b < \Delta z' < 0 \end{aligned}$$

while the longitudinal separation $\Delta x'$ is less critical due to slow vortex decay. It is thus the control objective to drive the follower UAS into this window and stay within in.

3.1 Input saturations

For a fixed-wing UAS, the maximum load factors are naturally limited by the maximum thrust of the engine and the aerodynamic parameters of the aircraft, such as the stall angle α_{max} as

$$|\mathbf{n}(t)| \leq \mathbf{N}(t) \quad (15)$$

These saturations are time-varying since, including the engine thrust, they are function of the dynamic pressure $\bar{q}(t) = \frac{1}{2}\rho(t)V_a^2(t)$.

3.2 Information constraints

It is assumed that observations of the relative position and relative velocity vector between each UAS and its predecessor are available.

This limitation allows to use low-cost vision-based relative localization techniques, which is a significant advantage taking into account the price range of GNSS Real Time Kinematics systems which would be required for localization with respect to the formation leader or other members of the formation that are now within the field of view of onboard vision sensors.

3.3 CSMC

It is the control objective to drive the system to the sliding surface defined by

$$\sigma(t) = \mathbf{G}\mathbf{x}(t) \quad (16)$$

$$\mathbf{x}(t) = \begin{pmatrix} \Delta \mathbf{p}(t) \\ \Delta \mathbf{v}(t) \end{pmatrix} \quad (17)$$

and, once reached, to keep it on it for all subsequent times $t \geq t^*$. With

$$\mathbf{G} = [\mathbf{G}_1 \mathbf{G}_2] \quad (18)$$

the position error dynamics in sliding mode are

$$\mathbf{0} = [\mathbf{G}_1 \mathbf{G}_2] \begin{pmatrix} \Delta \mathbf{p}(t) \\ \Delta \mathbf{v}(t) \end{pmatrix} \quad (19)$$

$$\Delta \ddot{\mathbf{p}} = -\mathbf{G}_2^{-1} \mathbf{G}_1 \Delta \dot{\mathbf{p}} \quad (20)$$

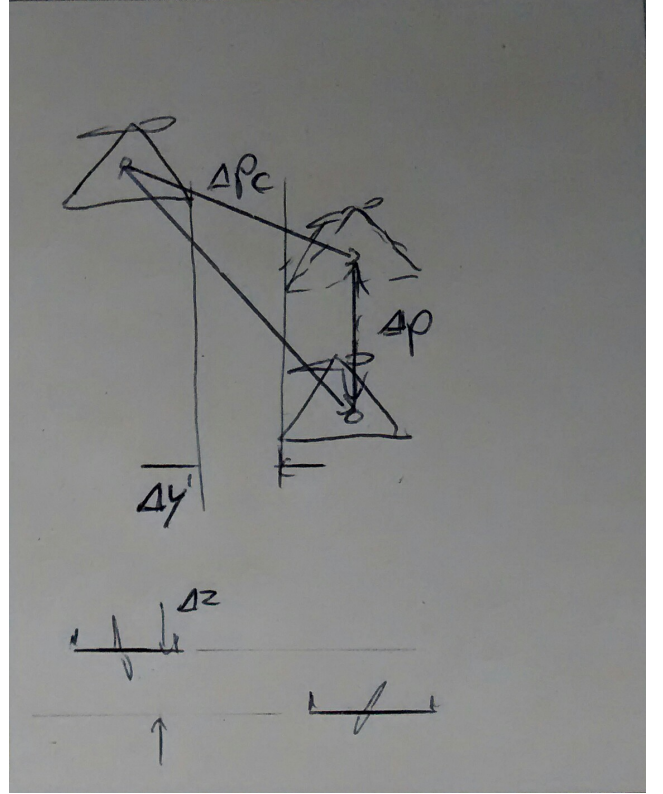


Fig. 2. Predecessor-follower geometry

Selecting $-\mathbf{G}_2^{-1} \mathbf{G}_1$ as Hurwitz ensures that $\Delta \mathbf{p}$ asymptotically converges to zero while in sliding mode.

Mesh stability is a feature of a three-dimensional formation of vehicles that allows separation errors to stay locally contained (see e.g. Pant et al. (2002)). In other words, separation errors between a pair of vehicles are not amplified towards the neighboring vehicle pairs. More vehicles can be added to a mesh stable formation without changing the local controllers, providing scalability. It is a well known fact (Pant et al. (2002)) that linear controllers with local feedback information are mesh unstable.

While in sliding mode, the position error dynamics are by definition confined to (20), independently of adjacent separation errors, implying mesh stability if the system can be kept in sliding mode.

The open loop sliding variable dynamics are

$$\dot{\sigma} = \mathbf{G} \begin{pmatrix} \Delta \mathbf{v} \\ \mathbf{u} + \mathbf{a}_{w,i} - \mathbf{a}_{i-1} - \Delta \ddot{\mathbf{p}}_c \end{pmatrix} \quad (21)$$

$$= \mathbf{G} \begin{pmatrix} \Delta \mathbf{v} \\ -\Delta \ddot{\mathbf{p}}_c \end{pmatrix} + \mathbf{G} \begin{bmatrix} \mathbf{0} \\ \mathbf{I} \end{bmatrix} (\mathbf{u} + \mathbf{a}_{w,i} + \mathbf{a}_{i-1}) \quad (22)$$

$$= \mathbf{G} \Phi_k + \mathbf{G} \mathbf{B}(\mathbf{u} + \Phi_u) \quad (23)$$

$$= \Phi'_k + \Phi'_u + \mathbf{u}' \quad (24)$$

The desired relative position $\Delta \mathbf{p}_c$ and its second derivative are communicated to each follower. Accelerations of the predecessor \mathbf{a}_{k-1} as well as exogenous perturbations \mathbf{a}_w acting on the vehicle i are assumed to be unknown but bounded. For notational convenience they are lumped into the disturbance vector Φ_u .

$$\Phi_u = \mathbf{a}_{w,i} - \mathbf{a}_{i-1} \quad (25)$$

while the known perturbations $\Delta \ddot{\mathbf{p}}_c$ are redefined as Φ_k

$$\Phi_k = \begin{pmatrix} \Delta \mathbf{v} \\ -\Delta \ddot{\mathbf{p}}_c \end{pmatrix} \quad (26)$$

further defining

$$\mathbf{u}' = \mathbf{G}\mathbf{B}\mathbf{u} \quad (27)$$

$$\Phi'_k = \mathbf{G}\Phi_k \quad (28)$$

$$\Phi'_u = \mathbf{G}\mathbf{B}\Phi_u \quad (29)$$

Note that all perturbations are assumed to satisfy the matching condition. The three axes are considered decoupled by the inner load factor controllers, allowing for SISO design.

Saturations on the virtual control input (27) can be derived from (15) as

$$|\mathbf{u}'| \leq \mathbf{U}' \quad (30)$$

$$\mathbf{U}' = \mathbf{G}\mathbf{B}\mathbf{R}_{eb}|\mathbf{g}|(\mathbf{N} - \mathbf{n}_{c,0}) \quad (31)$$

Since the inner loop load factor controllers cannot track discontinuous reference signals, a continuous control signal is mandatory. The system (23) is of relative degree $\mathbf{r} = (1 \ 1 \ 1)^T$, thus continuous-time Super-Twisting Sliding Mode controllers (CSTSMC, see e.g. Shtessel et al. (2014)) can be applied, providing continuous control signals. We apply the controller presented in Galzi and Shtessel (2006) extending it trivially from 2D to 3D tracking. The CSTSMC controller is then given by

$$u'_p = \alpha_p |\sigma_p|^{1/2} \text{sign}(\sigma_p) + \beta_p \int \text{sign}(\sigma_p) dt \quad (32)$$

where $p = 1...3$ indicates the three decoupled axes. Adding a term that eliminates the known disturbances $\Phi'_{k,i}$ as in Galzi and Shtessel (2006)

$$u'_p = \alpha_p |\sigma_p|^{1/2} \text{sign}(\sigma_p) + \beta_p \int \text{sign}(\sigma_p) dt - \Phi'_{k,p} \quad (33)$$

leads to closed loop σ dynamics of

$$\dot{\sigma}_p = \alpha_p |\sigma_p|^{1/2} \text{sign}(\sigma_p) + \beta_p \int \text{sign}(\sigma_p) dt + \Phi'_{u,p} \quad (34)$$

Provided the disturbances $\Phi'_{u,p}$ are bounded by $\Phi'_{u,p} \leq L_p$ controller parameters that fulfill

$$\alpha_p = 1.5\sqrt{L_p} \quad (35)$$

$$\beta_p = 1.1L_p \quad (36)$$

drive the system into 2-sliding mode, i.e. $\dot{\sigma} = \sigma = 0$ in finite time. The reaching time is bounded by $t_p^* \leq \frac{7.6\sigma_p(0)}{\beta_p - L_p}$, see Galzi and Shtessel (2006).

The actual control input \mathbf{n}_c is computed from (27, 5) as

$$\mathbf{n}_c = \frac{1}{|\mathbf{g}|} \mathbf{R}_{be}(\mathbf{G}\mathbf{B})^{-1} \mathbf{u}' + \mathbf{n}_{c,0} \quad (37)$$

using $\mathbf{R}_{eb}^{-1} = \mathbf{R}_{eb}^T = \mathbf{R}_{be}$

Discretization For implementation, the CSTSMC is sampled with a zero-order hold scheme. There are results for homogeneous sliding controllers such as the CSTSMC (see Shtessel et al. (2014)) stating that the error introduced by discrete sampling is quadratically proportional to the sampling time, i.e. $\sigma = O(T^2)$. Our simulation results confirm this, see section 4.

3.4 DSMC

Designing a sliding mode controller in the discrete time domain allows to take sampling time effects into account right from the beginning.

The σ dynamics assuming forward Euler discretization are

$$\sigma(k+1) = \sigma(k) + T(\Phi'_k(k) + \Phi'_u(k) + \mathbf{u}'(k)) \quad (38)$$

Since a discrete controller has no control over what happens to the continuous system between sampling instants, ideal sliding mode is not achievable. It is however possible to drive the system into so-called quasi-sliding mode, defined by the control objective

$$|\sigma_i(k)| \leq \epsilon_i \quad (39)$$

for $i = 1...3$, for all $k \geq k^*$ where ϵ is the width of the quasi-sliding mode boundary layer and k^* is the first sample for which eq. 39 is satisfied, i.e. when the system transitions from the reaching phase into quasi-sliding mode. The proposed DSMC is based on ideas presented by the authors of Monsees and Scherpen (2001). The following simple linear reaching law (proposed e.g. by Spurgeon (1992)) ensures asymptotic convergence to the sliding surface

$$\sigma(k+1) = \Psi \sigma(k) \quad (40)$$

with a diagonal $\Psi \in \mathbb{R}^{3 \times 3}$, $0 < \Psi_{i,i} < 1$ for $i = 1...3$. The choice of Ψ allows to trade off control effort and reaching time. Since (40) is equivalent to

$$|\sigma(k+1)| = \Psi |\sigma(k)| \quad (41)$$

the norm of the sliding variable decreases with every time step, indicating convergence to the sliding surface.

Remark As mentioned in Monsees and Scherpen (2001), a Lyapunov function does not - as in the continuous case - provide enough constraints to drive the system to the sliding surface without overshoot. This is due to the fact that a Lyapunov function only constrains the direction of the system's motion - towards the sliding surface - but not the magnitude of the next discrete step towards it.

The control input $\mathbf{u}(k)$ required to drive the system (38) according to the reaching law (40) can be computed from the open-loop σ dynamics to

$$\mathbf{u}'(k) = \frac{1}{T}(\Psi - \mathbf{I})\sigma(k) - \Phi'_k - \tilde{\Phi}'_u \quad (42)$$

Note that $\mathbf{u}'(k)$ contains an estimate of the unknown perturbations $\tilde{\Phi}'_u(k) = \Phi'_u(k) + \Delta\Phi'_u(k)$. Closing the loop, one obtains

$$\sigma(k+1) = \Psi\sigma(k) + T(\Delta\Phi'_u(k)) \quad (43)$$

Note that the reaching law (40) can not be followed due to the estimation error $\Delta\Phi'_u(k)$. Instead, assuming that initially the system is outside the quasi-sliding mode band, it will approach the sliding surface at least as long as

$$\Psi\sigma(k) \geq T(\Delta\Phi'_u(k)) \quad (44)$$

This defines the maximum boundary layer thickness as

$$\epsilon = \Psi^{-1}T(\Delta\Phi'_u(k)) \quad (45)$$

A simple way to obtain an estimate of the unknown disturbances is from the previous sample by

$$\Phi'_u(k-1) = \sigma(k) - \sigma(k-1) - T(\Phi'_k(k-1) + \mathbf{u}'(k-1)) \quad (46)$$

assuming that the disturbance rate is bounded by $|\frac{d\Phi'}{dt}| \leq \delta\Phi'$, assuming $\Phi'(k) = \Phi'(k-1)$ and a first-order approximation introduces an error $\Delta\Phi'_u(k)$ that is bounded by $|\Delta\Phi'_u(k)| \leq T\delta\Phi'$.

Note that with (45), the boundary layer thickness depends quadratically on the sampling time.

4. SIMULATIONS

Both controllers have been evaluated in a simulation environment. In all cases, the vehicle dynamics have been integrated with a forward Euler scheme at a sampling time of $t_{sim} = 10^{-4} s$, while the controller sampling time has been varied. While three-dimensional predecessor tracking is performed, only the vertical channel Δp_3 is considered here for clarity.

4.1 Controller parameters

For the CSTSMC, the controller gains are computed according to (35, 36), requiring the bounds L_i on the maximum unknown perturbations $\Phi'_{u,i}$ which are driven by exogenous disturbances $a_{w,i}$ and acceleration of the predecessor $a_{k-1,i}$.

These being bounded by

$$|a_{w,p}| \leq A_{w,p} \quad (47)$$

$$|a_{i-1,p}| \leq A_{i-1,p} \quad (48)$$

for $i = 1...3$, the bounds on $|a_{w,i}|$ have been obtained empirically from a time series representing 1h of simulated Dryden turbulence at the position of maximum incremental lift in the predecessor's wake filtered by closed loop

inner load factor controllers.

The bounds $A_{k-1,i}$ are less obvious, since they depend on the closed-loop behavior of the predecessor. Assuming that the control inputs of the predecessor stay within their saturation limits, i.e.

$$-U_i < \mathbf{u}_{i-1,p} < U_i \quad (49)$$

Now since

$$\mathbf{a}_{i-1} = \mathbf{u}_{i-1} + \mathbf{a}_{w,i-1} \quad (50)$$

\mathbf{a}_{i-1} is bounded by

$$|a_{i-1,p}| \leq U_p + A_{w,p} \quad (51)$$

leading to

$$L_p = U_p + 2A_{w,p} \quad (52)$$

Remark: From (52) it becomes clear that no guarantees can be given for the system to stay in sliding mode at all times under the assumption 49. This is due to the fact that the assumption 49 allows the predecessor $i-1$ to apply maximum accelerations that, if at the same time disturbances $\mathbf{a}_{w,p}$ act on the predecessor, cannot be followed by the follower i . Formally this can be checked by computing the equivalent control and its bounds that result from the sliding condition $\dot{\sigma} = \mathbf{0}$ as

$$u'_{eq,p} = -\Phi'_{k,p} - \Phi'_{u,p} \quad (53)$$

$$|u'_{eq,p}| \leq \Phi'_{k,p,max} + L_p \quad (54)$$

$$\leq \Phi'_{k,p,max} + U_p + 2A_{w,p} \quad (55)$$

Note that the bounds on $u_{eq,p}$ exceed the control saturations U_p .

For the first vehicle pair, which is formed by the virtual leader and the first aircraft, the predecessor control input bounds expressed by (49) can easily be tightened by limiting the second derivative of the virtual leader's trajectory.

!!!Explain what happens to following pairs, since control input of i becomes predecessor commanded acceleration of $i+1$ -; fundamentally not mesh stable. Expected result: tracking accuracy can be guaranteed for a certain number of pairs, once exceeded, controls saturate

For the DSMC, the entries of the reaching rate matrix Ψ are selected on line to stay within control input limits given the initial error state.

4.2 Disturbance models

Wake vortex disturbances A variety of approaches has been proposed to simulate the effects of wake trailing vortices on following UAS, mostly based on modified Horseshoe Vortex Models (HVM) (!!!cite) or Vortex Lattice methods (VLM) (!!!cite). For the purpose of this work, a HVM with modified core model presented in (Dogan et al. (2005)) is used. It is reported to provide predictions that are in good agreement of both VLM models and wind tunnel measurements while being of

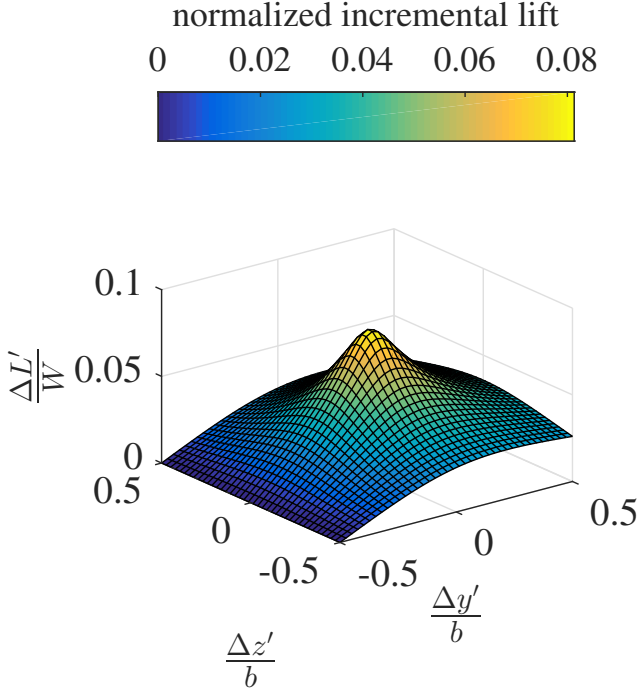


Fig. 3. Normalized incremental lift predicted by modified Horseshoe Vortex Model for $\Delta x' = 2b$. Note that $\Delta x'$, $\Delta y'$, $\Delta z'$ are wingtip to wingtip separations

great simplicity. In the vertical channel, the model predicts incremental aerodynamic lift perturbations as a function of the separation vector between a UAS and its predecessor, see fig. 3.

Atmospheric turbulence Atmospheric turbulence time series are generated according to the Dryden turbulence spectrum. The induced velocities are filtered by transfer functions corresponding to closed loop LQR load factor controllers designed for a small UAS ($b = 2.6m$).

Maneuver

REFERENCES

- Dogan, A., Venkataramanan, S., and Blake, W. (2005). Modeling of aerodynamic coupling between aircraft in close proximity. *Journal of Aircraft*, 42(4), 941–955.
- Galzi, D. and Shtessel, Y. (2006). Uav formations control using high order sliding modes. In *American Control Conference, 2006*, 6–pp. IEEE.
- Hummel, D. (1982). Aerodynamic aspects of formation flight in birds. *Journal of theoretical Biology*.
- Jake, V., Ray, R., Ennix, K., and Walsh, K. (2003). F/a-18 performance benefits measured during the autonomous formation flight project. Technical report, NASA/TM-2002-210732, Sept.
- Monsees, G. and Scherpen, J. (2001). Discrete-time sliding mode control with a disturbance estimator. In *Proceedings of the European Control Conference*, 3270–3275.
- Pant, A., Seiler, P., and Hedrick, K. (2002). Mesh stability of look-ahead interconnected systems. *IEEE Transactions on Automatic Control*, 47(2), 403–407.
- Shtessel, Y., Edwards, C., Fridman, L., and Levant, A. (2014). *Sliding mode control and observation*. Springer.

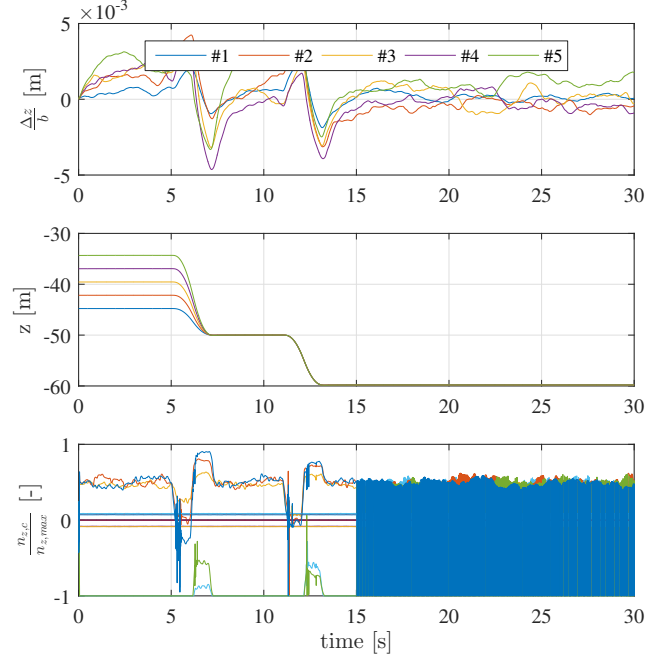


Fig. 4. CSMC controller $10^{-3}s$ sampling time

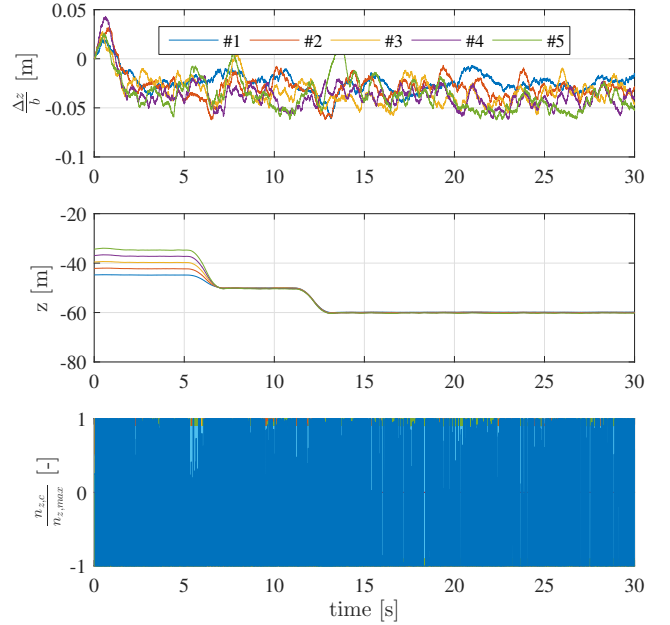


Fig. 5. CSMC controller $10^{-2}s$ sampling time

- Spurgeon, S. (1992). Hyperplane design techniques for discrete-time variable structure control systems. *International Journal of Control*, 55(2), 445–456.

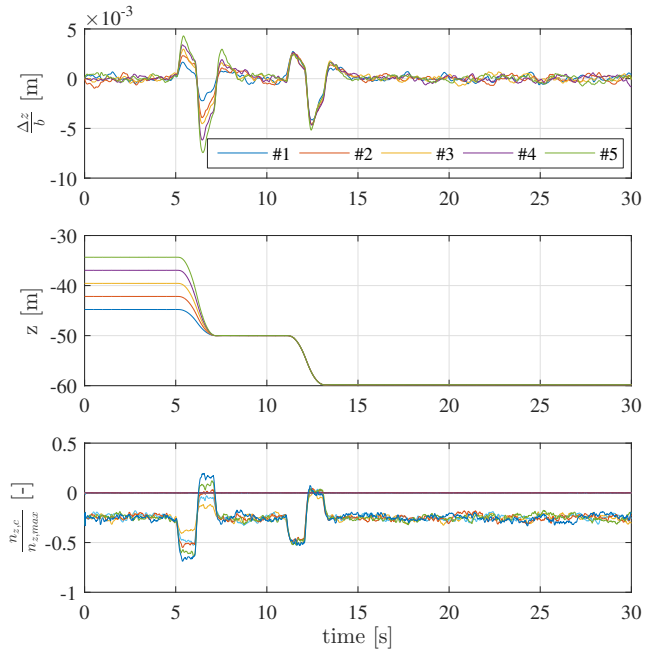


Fig. 6. DSMC controller 10^{-2} s sampling time

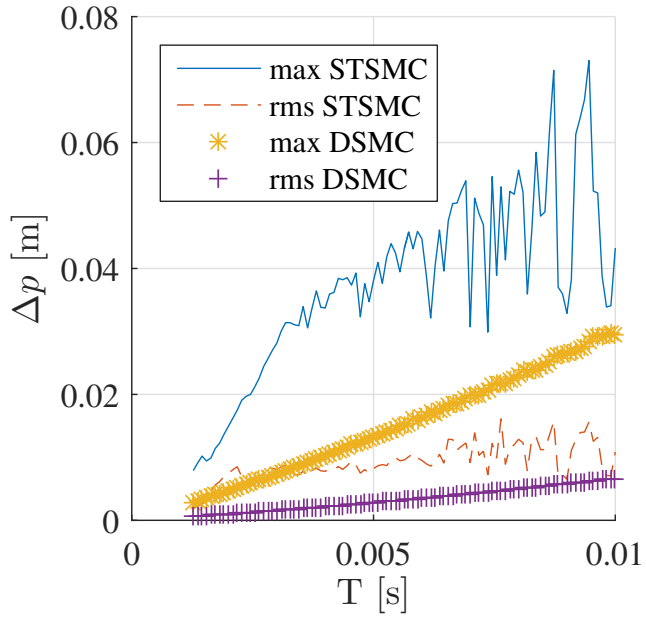


Fig. 7. Vertical position error measures vs. controller sampling time for CSTSMC and DSMC